Observations of dune interactions from DEMs using through-water Structure from Motion

Renske C. Terwisscha van Scheltinga [a,*], Giovanni Coco [b], Maarten G. Kleinhans [c], Heide Friedrich [a]

[a] Department of Civil and Environmental Engineering, University of Auckland, Auckland, New Zealand
[b] School of Environment, University of Auckland, Auckland, New Zealand
[c] Department of Physical Geography, Utrecht University, Utrecht, the Netherlands

ARTICLE INFO

ABSTRACT

The role of three-dimensionality (3D) in modulating both flow and sediment transport remains poorly understood. 3D bed elevation measurements are difficult to obtain due to irregular dune shapes and submergence. Using photogrammetric tools for topographic reconstruction has become popular in surface studies, yet water refraction makes through-water image capturing of submerged dunes still challenging. We show that through-water images and Structure from Motion (SfM) tools can produce accurate Digital Elevation Models (DEMs) of a measured dune field, with a high level of detail. It is a low-cost and non-intrusive alternative for submerged bed elevation measurements. We provide a detailed SfM workflow, introduce and discuss the use of camera coordinates and underwater ground control points, and processing steps needed to obtain high accuracy DEMs. Our method results in DEMs with mm resolution in controlled laboratory conditions. New data for 23 dune field DEMs from 6 experiments were obtained and are presented.

The dune field DEM time series provide insights on dune interaction processes. In our experiments, merging and defect creation were most common. Merging decreases the number of bedforms, and defect creation is responsible for more bedforms. Dunes continue to interact and jostle after achieving equilibrium. Simple crests are much more frequently observed than irregular, sinuous or double crests. Two-dimensional (2D) crest shapes were observed, although crest shapes were generally of 3D nature. Observed dune migration rates are not steady and vary in time and space. Bedform splitting speeds up dune migration, whilst neighbouring dunes tend to accelerate or decelerate. We identify a cascade of processes and show that 3D DEMs at high frequency are required to resolve observed rapid deformations and interaction of dunes. The identified dune interaction processes are inherent to sediment flux (variability), whereas the temporal component of the underlying sediment transport processes is still not well understood in relation to average transport.

© 2020 Elsevier B.V. All rights reserved.

1. Introduction

1.1. Background

Dunes are prominent features in alluvial rivers, such as the Mississippi, Jamuna (lower stream of the Brahmaputra), Parana, Zaire and Rhine river (Julien and Klaassen, 1995), among others. The growth and decay of dunes controls flood characteristics, with the shape and size of the dunes affecting energy decay. Compared to flat beds, dunes increase turbulent flow features, and the resistance of the flow. The form friction of bedforms generates a shear layer, along which turbulence is produced (Kwoll et al., 2017; Venditti and Bennett, 2000). In turbulent flow, energy is maintained by the mechanism of (rotating) eddy diffusion, ultimately breaking down into smaller vortices, whilst dissipating energy (Dey, 2014; Matthes, 1947). Most of the energy is dissipated in and near the wake region behind a dune crest (Venditti and Bennett, 2000). The total shear stress is larger over dunes, as compared to flat beds, and Lefebvre et al. (2016) measured relative increases from 1 to 1.9 with an increase in slip face angle. Large-scale coherent flow structures are initiated by vortices in the dune lee, which further affect mixing and sediment transport and are most developed for steep lee slopes (Kwoll et al., 2017). Permanent flow separation is observed at lee slopes steeper than 11–18° (Lefebvre et al., 2016), as is commonly encountered in shallow flows. This implies that dune shape has a major impact on energy decay. Recent simulations using 3D dune beds relate the presence and size of the flow separation zone and the wake, to the presence and properties of the slip face, as compared to the crest line or bedform height (Lefebvre, 2019). Approximations of the presence and size of reverse flow and wake can be derived from a bathymetric map (Lefebvre, 2019).

* Corresponding author.
E-mail address: rgal477@aucklanduni.ac.nz (R.C. Terwisscha van Scheltinga).

Mapping dunes is not only important for assessing hydraulic resistance. Sequential bathymetric data are a viable means to measure bedload transport in rivers (Abraham et al., 2011; Frings and Kleinhans, 2008; Nittrouer et al., 2008; Simons et al., 1965; Wilbers and Ten Brinke, 2003). For dune tracking methods to be valid, it is essential that the dunes migrate without changes in size, shape or spacing. However, dunes continue to interact and jostle after a statistical stable value of e.g. dune height has been reached 'at a point' and this is referred to as 'equilibrium' (Coleman and Melville, 1996; Jerolmack and Mohrig, 2005b; Reesink et al., 2018). The behaviour is called active deformation (McElroy and Mohrig, 2009). A relationship between the transport stage and deformation rate exists (Venditti et al., 2016). At the bedload dominated stage, the contribution of translation-related and deformation-related flux to the total flux is equal. As the transport rate increases, and dunes get bigger and move faster, the fraction of the total load contributed by translation increases and the fraction contributed by deformation declines. Thus, we know that dune deformation cannot be neglected as a contributing factor to the sediment fluxes driven by dune migration, with dune deformation impacting dune spacing and shape. Sediment transport is typically set as a steady flux by reach-averaged flow conditions and an open question remains whether sediment transport over dune-covered river beds is perhaps better described as the sum of changing, local, form flow interactions (Reesink et al., 2018).

Currently, we still have a limited understanding of the processes that determine dune deformation. Dune analysis has generally been based on assumption of essentially 2D dune morphologies, with the 3D shape or crest curvature being neglected. In order to unravel the components of migration and deformation of dunes for a variable dune field, bed elevation data for repeated transects are needed at much larger spatiotemporal resolution than usually collected in the past.

1.2. River bed mapping techniques

Underwater bedforms are typically mapped using submersible sonar (echo-sounding) transducers (Abraham et al., 2011; Friedrich et al., 2008; Guala et al., 2014; Parsons et al., 2005; Qin et al., 2015; Singh and Foufoula-Georgiou, 2013; Venditti et al., 2016) and conductivity sensors (Blom et al., 2003). These methods are characterised by low point density and a non-continuous representation of the bed. As an alternative, remote sensing techniques, such as LiDAR (Light Detection And Ranging), laser scanning, image spectral depth and photogrammetry are available since the 1970's (Fig. 1). They provide high precision maps of river topography (Alho et al., 2009; Javernick et al., 2014; Lane et al., 1994; Lane et al., 2003) and, less common, of submerged river beds (Kinzel et al., 2007; Westaway et al., 2001; Woodget et al., 2015). River beds with bedforms have high turbidity and poor visibility from suspended sediment, which makes photogrammetry, image spectral depth and laser scanning less suitable as a method for bathymetric mapping of natural sandy rivers compared to mapping of (shallow) gravel-bed rivers. Nonetheless, photogrammetry is time and cost-effective compared to other mapping techniques (Fryer, 1983; Lane et al., 2010; Woodget et al., 2015). Since 2010, Structure from Motion (SfM) has become hugely popular as a method of photogrammetry to measure 3D topography (Mosbrucker et al., 2017; Westoby et al., 2012). In SfM, a 3D structure is rebuilt from a set of overlapping images. This is achieved by moving the camera between image capturing to give the images an offset, as in photogrammetry, but SfM is simpler in setup and faster to process, using iterative bundle adjustment to match pairs (Westoby et al., 2012). Computational procedures in SfM are performed within the software, and the actual codes are not accessible, resulting in part of the workflow being a black box.

1.3. Through-water photogrammetry

Mapping of submerged topography by photogrammetry requires a correction for refraction at air-water interface: when the camera lens is directly above each image point, true depth can be estimated by multiplying the apparent depth by 134% (assuming a refraction index of 1.33) (Fryer, 1983; Westaway et al., 2001). First, Westaway et al. (2001) produced a raw uncorrected DEM that allowed mapping the elevations at the water edge into a map of water surface elevation. Subtraction of the map of water surface elevation with the uncorrected DEM provided an apparent water depth map, which was multiplied by the refraction correction into a map of real water depth. Subtraction of the water surface elevation map with the map of real water depth gave a submerged bed elevation map that was merged with the DEM of the dry topography into a DEM of dry and submerged river topography. Comparison of measured depth with a total station and automatic data logger showed increasing errors with increasing water depth, and mean error of 0.010–0.105 m and standard deviation of 0.092–0.116 m. Errors were large beyond 0.4 m water depth. Further development of photogrammetry to measure submerged topography was done by Woodget et al. (2015) using an unmanned aerial system for image capturing, whilst DEMs were processed with SfM photogrammetry. The same procedure for the refraction correction as Westaway et al. (2001) was applied. Validation with total station measurements showed increasing errors with water depth, and a dome-like deformation of the DEM for an otherwise flat surface (Woodget et al., 2015). They compared their DEMs (with refraction correction) with DEMs from bathymetric laser scanning, digital photogrammetry and a spectral depth method and reported finer resolution (0.02 m) with lower mean errors (0.004–0.006 m). A significant improvement to the 'simple' refraction correction of Westaway et al. (2001) was made by iterating through all possible point-camera combinations in the SfM reconstruction using a custom script that reads point cloud, camera positions/orientations, and camera sensor parameters (Dietrich, 2017; Kasvi et al., 2019).

Refraction correction on the images can be also applied before 3D reconstruction, but tests showed that enhancement and correction methods did not improve feature detection and overall 3D reconstruction in the specific SfM – MVS software (Agrafiotis et al., 2017). Machine learning tools were also used to overcome the water refraction errors by comparison to LiDAR surveys (of the seabed) (Agrafiotis et al., 2019; Skarlatos and Agrafiotis, 2018). 'Underwater ground control points' are introduced automatically, to learn the systematic underestimation of the estimated depths. This avoids the need for camera orientation and intrinsic parameters (Agrafiotis et al., 2019; Skarlatos and Agrafiotis, 2018). Comparison of the predicted and apparent water depth showed that most points are concentrated in a narrow distribution of a linear shape at water depths of 0–15 m, and a coefficient of 1.5–1.6, depending on the data set and intersecting at roughly the mean topographical height (Agrafiotis et al., 2019).

In the present work, we further explore using SfM-MVS on through-water images for application in the laboratory (where underwater ground control points are available and water clarity can be controlled). Successful application of SfM on through-water images makes it possible to study in detail previously inaccessible 3D dynamics of dune deformation and translation.

1.4. Dune interaction processes

Kocurek et al. (2010) identified dune deformation processes and classified them into a spectrum from constructive to regenerative interactions that drive pattern development for Aeolian and aquatic dunes. Constructive interactions transform the dune field toward fewer, larger and more widely spaced dunes. Regenerative interactions transform the dune field toward a state with more crestlines. In Table 1, a description of dune interaction processes is presented that are relevant to this study. A defect is here defined as a break or irregularity in the pattern, e.g. crest terminations. Defects and whole bedforms interact and a simplified defect model for Aeolian transport conditions indicates that the pattern dynamics follow the defect dynamics (Werner and Kocurek, 1997). Most interactions are understood only in a rudimentary way
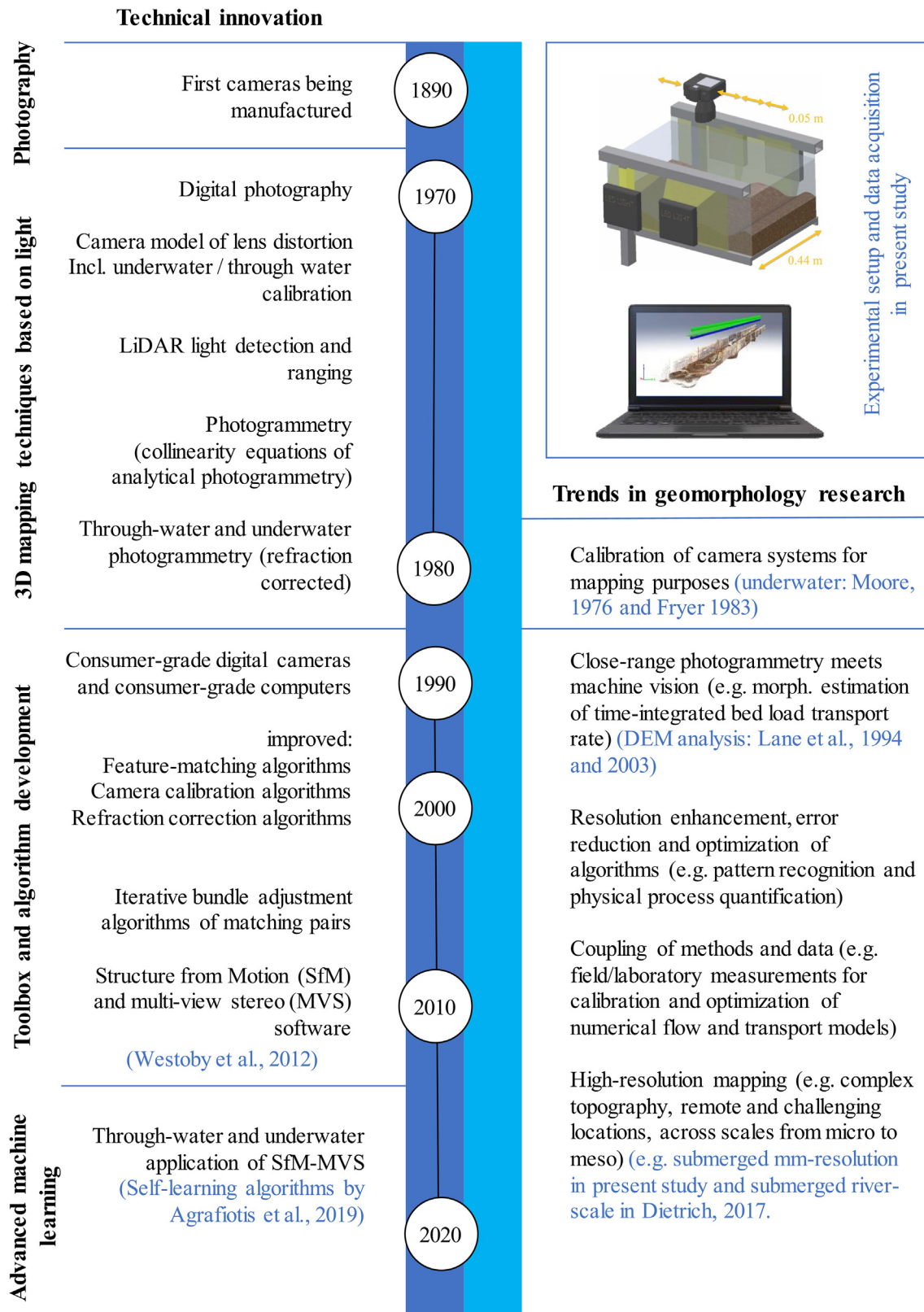
Technical innovation

Photography

First cameras being manufactured — 1890

3D mapping techniques based on light

Digital photography — 1970

Camera model of lens distortion Incl. underwater / through water calibration

LiDAR light detection and ranging

Photogrammetry (collinearity equations of analytical photogrammetry)

Through-water and underwater photogrammetry (refraction corrected) — 1980

Toolbox and algorithm development

Consumer-grade digital cameras and consumer-grade computers — 1990

improved:
Feature-matching algorithms
Camera calibration algorithms
Refraction correction algorithms — 2000

Iterative bundle adjustment algorithms of matching pairs

Structure from Motion (SfM) and multi-view stereo (MVS) software
(Westoby et al., 2012) — 2010

Advanced machine learning

Through-water and underwater application of SfM-MVS
(Self-learning algorithms by Agrafiotis et al., 2019) — 2020

Experimental setup and data acquisition in present study

0.05 m

0.44 m

Trends in geomorphology research

Calibration of camera systems for mapping purposes (underwater: Moore, 1976 and Fryer 1983)

Close-range photogrammetry meets machine vision (e.g. morph. estimation of time-integrated bed load transport rate) (DEM analysis: Lane et al., 1994 and 2003)

Resolution enhancement, error reduction and optimization of algorithms (e.g. pattern recognition and physical process quantification)

Coupling of methods and data (e.g. field/laboratory measurements for calibration and optimization of numerical flow and transport models)

High-resolution mapping (e.g. complex topography, remote and challenging locations, across scales from micro to meso) (e.g. submerged mm-resolution in present study and submerged river-scale in Dietrich, 2017.

Fig. 1. Photography has been an important tool for data acquisition in geomorphology research since the availability of cameras. 3D mapping techniques based on photogrammetry in underwater conditions were developed in 1970–1980. After availability of consumer grade digital cameras and computers from 1990, improvements of algorithms and toolboxes has allowed current high-resolution mapping of the complex topography of submerged river beds from grain to reach-scale. Figure inset is representing the experimental setup.

and (i) exploration of the stages in the development of specific dune interactions and (ii) the impact of specific interactions upon measurable pattern parameters, such as spacing and crest length, have not been extensively investigated (Kocurek et al., 2010). A spectral analysis approach gives insight into different bedform scales in a dune field, assuming steady state. Guala et al. (2014) use 2D spectral analysis to show that

Table 1
Dune and defect interactions relevant to our analysis, in alphabetical order. Identification is based on the descriptions and classification by Kocurek et al. (2010).

Observation	Process	Description
Merging type I (cannibalization)	Constructive; whole-dune interaction	Complete destruction of the downstream dune by scour associated with a strong back eddy
Defect creation	Regenerative; defect interaction	The breakup of a dune crestline whereby it creates more individual defects (decreasing crest length, and increasing the number of defects/dunes)
Defect/bedform repulsion	Whole-dune and defect interaction	The crestline of an approaching defect/dune merges with the crestline of the target dune/defect. The remnant crestline of the downstream dune then breaks and migrates away as a separate dune/defect, with characteristic trailing arms. These new defects, however, migrate faster than the core dune/defect and once again become typical downstream extending features.
Lateral linking	Constructive; defect interaction	Lateral merging of defects, which lengthens crestlines, and reduces the number of defects (and defect density)
Merging type II (coalescence)	Constructive; whole-dune interaction	Two dunes combine into one. At the essence is a difference in migration speed of dunes (smaller dunes overtake and merge with slower, larger dunes). Merging is successful only where the approaching dune is significantly smaller than the target dune.
Splitting	Regenerative; whole-dune interaction	The emergence of a new dune upon a stoss slope that is extending and decreasing in slope. The new stoss slope grows to a size comparable to the original host dune.
Superposition	Defect interaction	Superposed sand waves remain as subordinate features on a stoss slope

different sizes of bedforms exist simultaneously. Smaller bedforms, generally assumed to be superposed on larger dunes, account for most of the transport (Guala et al., 2014). A relation between the length of the bedforms (sand waves) and their celerity exists. Smaller sand waves travel at faster speed than larger sand waves, resulting in interaction: e.g., a small wave will catch up with a large wave and subsequently 'cuts off' sediment supply from the large wave (Warmink et al., 2014). During this process, the large wave (temporarily) destabilizes, as the sediment load is no longer saturated at its crest (brink point). Superposition affects the rate of bedform migration and volume of sediment transported, resulting in flow field changes and interactions between bedforms, and vice versa (Best, 2005; Frings and Kleinhans, 2008; Kleinhans et al., 2007).

1.5. Objectives

In this study, we present a novel method for non-intrusive measurements of detailed dune Digital Elevation Models (DEMs), providing information on (i) the 3D topography of crests and (ii) the phenomenology of dune and defect interactions and (iii) the effect of dune interactions on dune migration. We provide a new method with sufficient resolution and the extra dimension (as opposed to profiles) to be able to gain better understanding of dune migration and deformation, and the relationship with average sediment transport. We validate the DEMs by comparing SfM through-water results to laser scanner measurements and drained flume in-air SfM measurement. Our study objectives are:

1. To provide solutions to use through-water images as input for SfM tools, to obtain accurate 3D bed geometry measurements in a laboratory flume.

2. To track dune interactions and their relation to crest deformation using DEMs and determine how dune interactions contribute to variations in dune crest migration.

2. Data collection

2.1. Experimental setup

The flume used is 11.9 m (m) long, 0.38 m deep and 0.44 m wide and recirculates water and sediment. The water level is controlled in the downstream tank with a sharp-crested weir. Water and sediment flow rates are controlled with a water and sediment pump, respectively, and the flume is operated under sloping conditions. The sediment mixture is a natural sand with median diameter of 0.75 mm and D10 and D90 of approximately 0.5 mm and 1.1 mm, respectively. Experimental parameters are provided in Table 2. Flume slope, water level and pump rates were chosen to generate uniform flow for flat-bed conditions. Once dunes developed and migrated, minor variations in water surface slope throughout the experiment were observed, due to the nature of dune dynamics. Velocity profiles (not presented) were measured with a Nortek Vectrino+ with 4 probes. Data collection of DEMs was performed after >14 h of experimental time to ensure equilibrium conditions, with variations for each experiment (Table 2). For some experiments, the flume was once drained and refilled to improve water clarity, with the flow resumed for at least 10 min before data collection re-started. Dune growth in similar condition of flow velocity (0.5 m/s) and water depth (0.15 m) was measured by Venditti et al. (2005), with dune height increasing until 3.5 h of experimental time, and dune length increasing until 8.5 h of experimental time (Flow A in their Fig. 3).

2.2. Camera setup

A Nikon D90 camera with an AF-S Nikkor 10 mm lens was placed on a movable carriage to collect overlapping images of the bed surface from top view (see inset in Fig. 1). A number of imaging and SfM tests were conducted and analysed to optimize the data acquisition. The image overlap along the flume between individual images was 0.05 m and each image captured 0.9 m of the sediment bed. The flow is paused to collect the images for SfM, at which stage a 1.2 m long perspex plate is put in place, not influencing dune formation development. Using a perspex plate improved the image pair matching and ensured negligible light refraction and reflection. The technique of using a perspex plate has been previously successfully applied for bedload measurements in free-surface conditions (Fathel et al., 2015; Heays et al., 2014; Terwisscha van Scheltinga et al., 2019). The covered area is of short length and sediment transport studies under ice-covered surface have shown that the lower layer in a covered flow can be treated as a free-surface flow for the purpose of calculating bedload transport (Lau and Krishnappan, 1985). We defined the streamwise coordinate origin (x = 0 m) as the location where we observed uniform flow, at which location the sediment bed extended already for 1.5 m. Data collection took place between x = 1–7 m, ensuring no upstream influence on dune formation by the outlet.

SfM data collection recommends using convergent case images to increase the accuracy of the retrieved DEM model (Mosbrucker et al., 2017) and decrease the systematic error of the dome-like feature. In our experimental setup, the camera is placed perpendicular to the flume slope. Recording images perpendicular to the flume ensures that (i) the number of pixels that cover the cross-stream width of the flume are a measure of bed elevation, providing extra validation of bed elevation of the obtained DEM models, (ii) the captured images can be used to track the crest shape, and (iii) application of the refraction correction is simplified. 23 sets of images were collected for six experimental runs, with runtimes of 11–22 min between recordings. Images to determine the accuracy of the DEMs were collected using in-air SfM.

Table 2

Experimental runs and parameters, and data collection summary. The run names indicate average flow velocity, water depth and initial flume slope.

Run name	Flow velocity (m/s)	Water depth (m)	Initial flume slope (-)	Bed slope from DEMs (-)	DEMs (#)	Exp. time between first and last DEM (minutes)	Exp. time (hours)	Dune migration (m/s)
FR051210	0.48	0.12	0.0010	0.0042	3	0	30	
FR051515	0.48	0.15	0.0015	0.0026	7	94	100	0.000343
FR051815	0.48	0.18	0.0015	0.0015	3	30	14	0.000166
FR051522	0.50	0.15	0.0022	0.0023	4	44	16	0.000400
FR061815	0.58	0.18	0.0015	−0.003	3	24	20	0.000505
FR071515	0.65	0.15	0.0015	0.0031	3	30	65	0.000647

2.3. Camera calibration

In-air and through-water images were calibrated for radial and tangential lens distortion using a checkerboard (Lavest et al., 2003; Li et al., 2016; Moore, 1976; Shortis, 2015). The lens has a short focal length, which enhances the perspective more strongly. However, due to submergence, the increase in focal length counterbalances the perspective change and results in a small lens distortion for the used camera and experimental setup. This effect was described by Moore (1976). Since the lens distortion is small, potential errors resulting from non-optimized internal camera parameters are small as well. Our preliminary testing showed that the change in results is negligible if sensitivity to submergence and variations between repeated calibration sets were corrected for. Due to the minimal observed errors, we do no compensate for the tangential components of the distortion model.

3. SfM for through-water images

In SfM, a 3D structure is rebuilt from a set of overlapping images. SfM generates 3D point clouds in the image space. To convert point clouds into an object space, a grid of ground control points (GCPs) or tie points with known coordinates needs to be defined. In our experimental setup, GCPs are the flume frames, located 0.88–0.92 m apart, with manually drawn (height) lines on the glass wall every 0.02 m. In general, due to the nature of the technique, SfM is accurate and the accuracy can be further increased by increasing image overlapping or moving the camera closer to the surface, or increasing the focal length (Ferreira et al., 2017). A texture is necessary to perform SfM (Morgan et al., 2017). Uniform sediment grains may induce poor detection and matching, as they are in similar size and colour. The sediment mixture in the presented experiments is a unimodal mixture that contains lighter and darker particles of different shapes and sizes. Thus, individual grains can be identified in the experiments' sand bed images, which benefits the application of SfM.

3.1. Data processing workflow

The 3D reconstruction is based on a suite of computational procedures. The commercial software Agisoft Photoscan is commonly used for SfM processing, containing all SfM procedures from cloud reconstruction to dense point cloud reconstruction, whilst proving functionality for displaying and meshing (Morgan et al., 2017). In this study however we used Pix4Dmapper, which we found to be of similar performance and flexibility than Agisoft Photoscan. The images are loaded into Pix4Dmapper (step 1 in Table 3) and the software output is a point cloud model (step 12 in Table 3), following the workflow as presented in Table 3. In comparison, for in-air conditions step 3, 4, 8 and 16 are not necessary.

3.2. Point cloud optimization

There are several challenges that affect the scaling of the point cloud to real coordinates, and thus the accuracy of the DEMs. Firstly, the apparent focal length of the lens changes for through-water conditions.

Compared to in-air conditions, the focal length increases for through-water images with a factor of 1.337 (Lavest et al., 2003) and is sensitive to relative distance of rays in water and in air (Skarlatos and Agrafiotis, 2018). The scaling of object distance to the sensor in SfM tools is based on in-air conditions (and depends on the sensor size, the focal length of the lens and the focal length multiplier). The length scale proposed during SfM processing is underestimated for through-water conditions. Secondly, the software aims to reoptimize the internal camera parameters. This option should be ignored, as it can introduce false correlations between focal length and radial components for the used lens distortion models. Only if SfM camera calibration algorithms programmed for submerged conditions become available, can that option be re-considered. The software uses an iterative procedure to optimize the match between matched points, camera parameters and the true scales based on the ground control points and camera coordinates. Errors are automatically introduced as the iteration assumes in-air conditions, while the matched points are submerged. A common result we found was model rotation, flipping and doming. Our workflow presented in Table 1 will increase the chance of the algorithm to produce the true topography. Essential to the success are georeferencing of the camera locations, the GCP's, and incorporating the submergence corrected focal length before initial processing. Recent updates of the Pix4D software incorporate settings that further facilitate the processing, e.g. All Prior Internal Camera Parameter Optimization, which reduces the tendency of flipping. Lastly, for some models, we observed a warp in the

Table 3

Pix4Dmapper processing steps and point cloud generation post-processing steps.

Step	Description
1.	Define a project in Pix4Dmapper
2.	Load images to the project
3.	Define internal camera parameters for submerged conditions
4.	Geo-locate the camera position of each image
5.	Incorporate 10 GCPs (1 per 0.9 m of flume length at both sides of the flume)
6.	Apply initial processing (feature detection, feature matching, automatic aerial triangulation and bundle block adjustment)
7.	Determine the accuracy of the initial processing from the quality report. Validation is done based on the accuracy of the transformation to real coordinates based on the GCPs.
8.	Add 4 GCPs at average bed elevation to prevent 'warping' and assure appropriate scaling of the mean bed level.
9.	Rematch the features
10.	Assess the performance of the initial processing. Possible errors are warping in the y-direction, warping in the x-direction, manual input error of GCPs or camera locations, inferior image quality (e.g. reduced sharpness, low contrast from suspended particles, and differences in illumination between images).
11.	Apply the dense point cloud reconstruction
12.	Export of the dense point cloud
13.	Filtering of the point cloud by excluding outliers and cutting the edges.
14.	Interpolation of the point cloud to a gridded map
15.	Applying correction for doming, if needed (not applied in present study). Output camera location file compared to input camera location file can be used as an approximation of the doming errors.
16.	Applying correction for submerged conditions, if needed. The correction is sensitive to water depth, software release, i.a. The refraction correction scales linearly with bed elevation relative to mean bed level.

longitudinal or cross-stream direction, which is related to the point cloud after initial processing. Step 10 (Table 1), adding GCP's at mean bed elevation, minimizes the tendency for warping. Thus, with the proposed workflow, after step 10 DEMs did not need a correction for warping.

3.3. Validation through comparison with in-air SfM and laser scanning

To determine the accuracy of the obtained DEMs from SfM on through-water images, a Leica terrestrial laser scanner was used to scan the sediment bed elevation of a bed covered with bedforms. The flume was drained slowly, avoiding particle displacement, to scan the sediment bed. Thereafter, overlapping images were captured for in-air SfM application. The DEMs of the same dune field, obtained with the three different techniques, are shown in Fig. 2A–C. The point cloud density of the laser scan was lower than the point cloud density from in-air SfM and from through-water SfM. Comparison between in-air SfM and laser scan and through-water SfM respectively, shows that most points are concentrated in a narrow distribution of a linear shape and deviations in the order of millimetres (Fig. 2 D–E). The validation shows that the representation of the dune bed is similar for the three methods, supporting the use of through-water SfM as a practical and accurate tool. For the various water depths used, linear bed elevation correction was applied as needed. Our experiments with 0.15 m mean water depth required a water refraction correction of factor 1.2, relative to the mean bed level. Our experiments with 0.18 m mean water depth did not require a water refraction correction. The use of correction factors to compensate for submersion is also described by Woodget et al. (2015), with their correction factor scaling with the refractive index of clear water, while in Agrafiotis et al. (2019) the correction factor is 1.5–1.6 relative to mean bed level. It is shown that a high point cloud density of the submerged bed is obtained using SfM and the retrieved DEM compares well with DEMs obtained with the two validation methods.

3.4. Effect of flume draining and refilling on the sediment bed

Verification was done to evaluate the level of detail in obtained DEMs from SfM on through-water images. The sediment bed from experiment FR051210 (Table 2) was used for the evaluation and the water depth was increased to 0.15 m for data acquisition. The top DEM in Fig. 3A shows the submerged condition with six dune crests over a length of 5 m, exhibiting steep lee slopes. Smaller superposed

features are visible on top of the dune slopes. Streamwise-oriented ridges exist in the trough regions. The dune crests have a lobe shape and there is a tendency for a cross-slope to exist. The middle DEM (Fig. 3A) is the drained condition (in-air SfM), showing agreement between the in-air and through-water DEM. Warping can be identified from quality assessment of the GCPs and is visible in the streamwise direction (Fig. 3B). In our workflow, we incorporate a correction for warping when GCP quality assessment indicates the need for it. The bottom DEM (Fig. 3A) is captured in submerged condition, after slowly refilling the flume. Fig. 3C shows the DEM of difference (DoD) between the top and bottom DEM. Drainage and refilling of the flume affects the sediment bed in the trough regions and affects the dune crests. Erosion of the crests and sediment redistribution at ridges in the trough is observed. In addition, visual observations confirmed that the identified sediment redistribution occurred mostly during refilling of the flume. It is shown that our through-water SfM method ensures an accurate representation of the topography of a sand bed covered with dunes and superposed features, and that draining and refilling of the flume for data collection purposes, as is a commonly used process, can be avoided with our proposed method, and with it associated sediment redistribution.

4. Dune translation and deformation

4.1. Dune crest shapes

An assumption that is commonly made when analysing repeated transects is that the dune crests are mainly 2D in shape. During the experiments we observed 2D crests, but also irregular and asymmetrical crests are commonly observed. For all experimental DEMs, the crest shapes are analysed and a classification of seven different shapes is made, as shown in Fig. 4. Most observations (30% frequency in Table 4) are of crests with an asymmetrically positioned lobe, when symmetry is considered along the centreline of the flume. Also, 2D straight crests and (symmetrical) lobe crests are observed frequently (37% of the dune crests). Other shapes are oblique crests, irregular crests, sinuous crests, and double crests. Deformation of crest shapes is observed between DEMs and suggests that crest deformation is common, though non-deforming crests also exist for the time ranges of the DEMs. Time series of dune migration and deformation longer than we recorded are needed, in order to describe the stages of crest deformation and their effect on measurable pattern parameters, such as crest length.
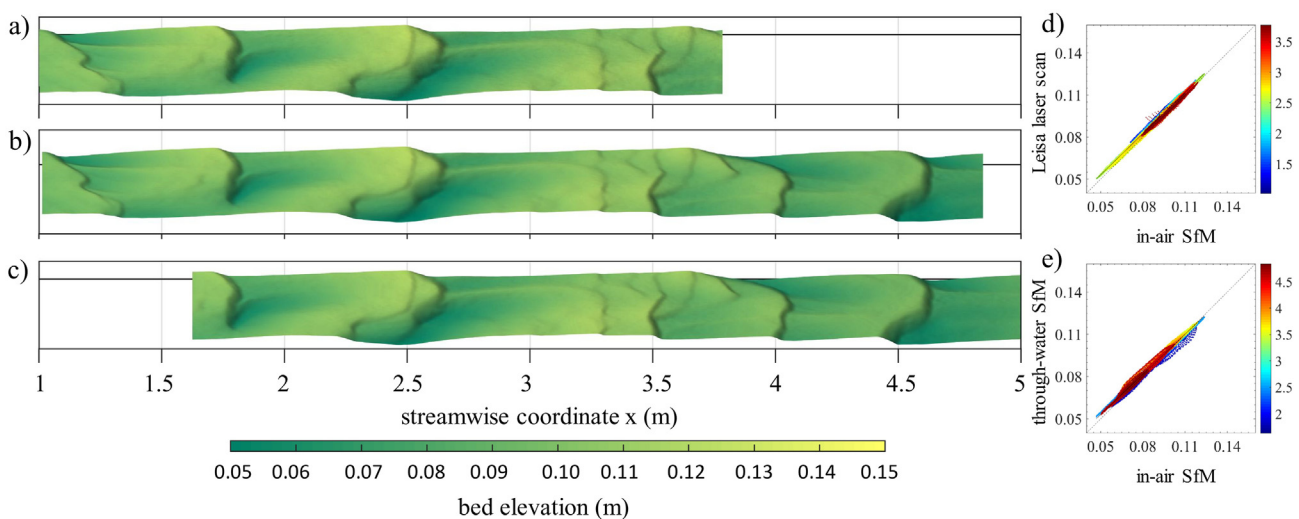

Fig. 2. Shadowed DEMs of the mobile sand bed covered with dunes. Measurements are from Leica laser scan (A), SfM processing of in-air conditions (B), and SfM processing for through-water images (C). Validation of the measurements is shown in (D) and (E). The colour scale represents the streamwise coordinate X (m). The measurements are interpreted on a 4 mm × 4 mm grid.
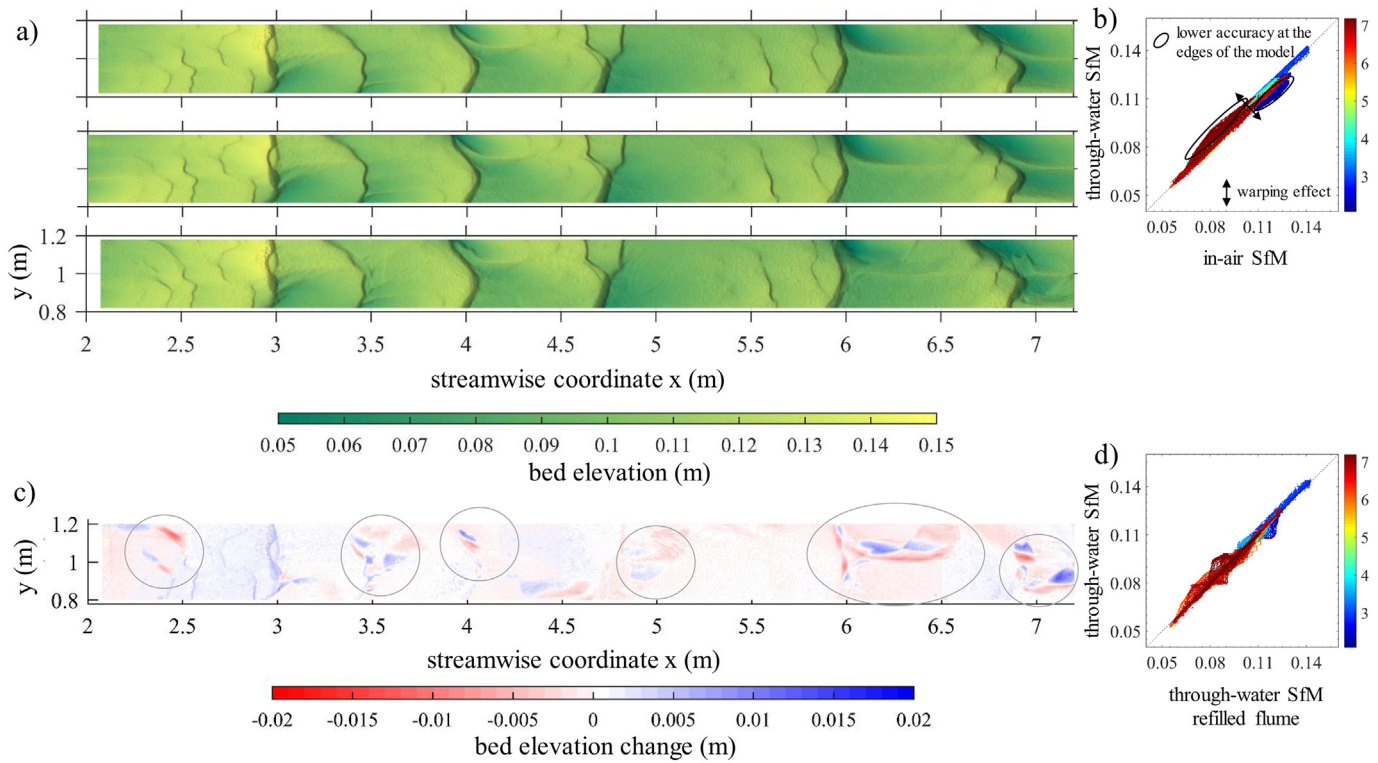
Fig. 3. DEMs of the sand bed with dunes from SfM processing of through-water images before and after draining the water from the flume and refilling the flume (A). The methodology is sensitive to 'warping' in the x and y direction (B). Observed x-warping error is ~1 mm per m. The DEM of difference shows local changes due to refilling the flume (C and D). The point density is approximately 1.5 point per mm^2 and the surface is presented by interpolation of points to a grid of 2 mm × 2 mm.

Fig. 4. Examples of crest shapes that were present in the experimental DEMs.

4.2. Observations of bedform interactions in the experiments

In the experiments, a range of dune interactions were observed, and the interactions are compiled in Fig. 5. The dune crests are aligned in subsequent DEMs to visualize the dune evolution. Whole dune interactions of bedform splitting and merging were observed, as well as defect interactions, such as defect creation, lateral linking, off-centre collision and defect migration. The interactions can be classified into 'regenerative' and 'constructive', according to the description by Kocurek et al. (2010). The sediment bed was deformed by processes from both classes. Whole dune interactions were captured in two to three DEMs, thus occurring within 12–30 min. Defect interactions were faster and were mostly only visible in one to two DEMs. Defects that propagated over long dunes, migrated and interacted faster than was traceable with the chosen timestep between the DEMs. More interactions occurred, but they could not be classified with the available data.

For experiment FR051515 (Fig. 6), seven subsequent DEMs were collected over 94 min. The average dune height is 0.030 m in the centre of the flume, using the bedform tracking tool (BBT) (van der Mark et al., 2008). The DEMs show migration of the dunes, as well as dune interactions. Small-scale features, superposed features, irregularities of the crests and ridges in the troughs are distinguished. The 3D data show there is a tendency of the crestlines to be curved or irregular, and that cross-slopes exist in the narrow flume (0.44 m wide). The topography development stages are traced, and the dune and defect interactions are classified in Fig. 6. The crest of the most upstream dune in the first DEM deforms during migration and shows splitting, defect creation and defect repulsion. The dune in the middle of the first DEM lengthens from 1.3 m ($t = 0$ min) to 2 m ($t = 64$ min), at the same time the upstream dune shows a sequence of evolution of defect creation, merging type I, defect creation and merging type II. Then, captured in the last DEM, the dune length shortens to 1.3 m, as lateral linking of defects takes place on the dune slope. The dune crest undergoes changes as
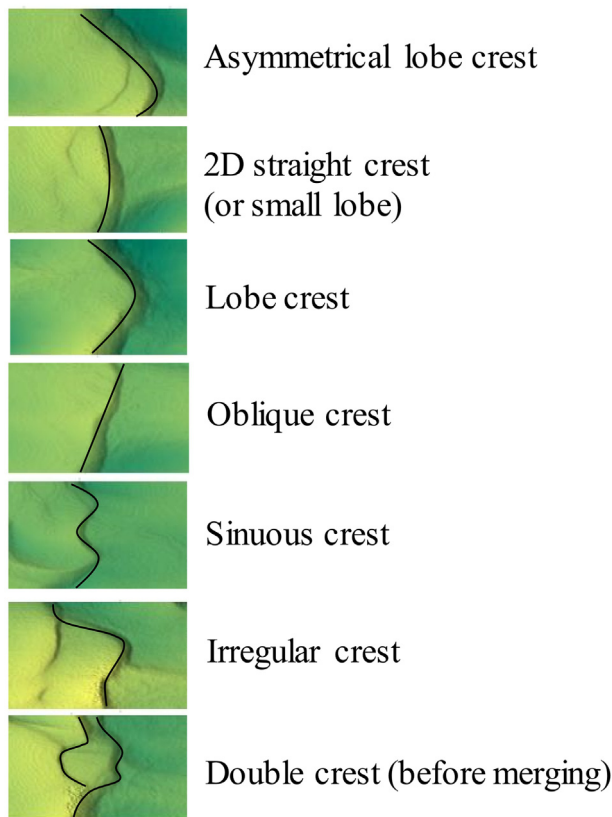
Table 4
Observations of crest shapes in the DEMs.

	FR051515	FR051522	FR051815	FR061815	FR071515	Sum	Relative frequency (-)
Asymmetrical lobe crest	10	8	6	4	3	31	0.30
Lobe crest	7	5	2	1	6	21	0.20
2D straight crest	5	6	2	3	2	18	0.17
Oblique crest	5	1		2	1	9	0.09
Irregular crest	6	2		2	2	12	0.12
Double crest	3	1	1	2	3	10	0.10
Sinuous crest	2	1				3	0.03
	38	24	11	14	17	104	1.00

well: crest deformation, lateral linking, merging type II and defect repulsion. The stages of evolution of the crest are influenced by defects on the stoss slope of the long dune. The third dune in the first DEM shortens from 1.3 m to approximately 0.5 m by merging.

A second set of four DEMs covering 45 min of dune migration, with a steeper bed slope (0.0022), is shown in Fig. 7. The upstream dune in the first DEM undergoes crest deformation, defect creation and merging type II. The merging process appears to slow down the dune migration here. The second dune shows merging (either type I or type II). The third and the fourth dune are of 0.8 m and 0.7 m length (top DEM) and merge into a 1 m long dune (bottom DEM). Before merging, the dune crest deforms, a defect is created, and lateral linking occurs.

4.3. General observations

The obtained DEM series' show that the interactions are quickly followed by other interactions. The dune and defect interactions that simultaneously occur upstream and downstream of a dune affect the spacing of the dune. For the series of seven and four DEMs, dune and defect interactions seldom occur independently, and it is challenging to define when a process starts, and when a process ends. Most common are merging type I and defect creation (Table 5), which are a constructive and a regenerative process. The results indicate the following general observations:

- Asymmetrical lobe crest is a common shape for a short dune (in the wake of a larger dune).
- A 2D straight crest is susceptible to defect interactions and the crest shape deforms easily.
- A double crest is a transitional shape, often related to merging type II (coalescence).
- Oblique, irregular and sinuous crests are often related to merging type I (cannibalization), defect creation and lateral linking and are actively deforming dune crests.
- An asymmetrical lobe crest is a stable crest shape and the shape can persist through 3 DEMs, or longer.
- Large (and long) dunes have several superposed bedforms on their stoss slope, and the crest shape is a simple form such as 2D straight, lobe crest or oblique crest while double crests occur as a transitional stage.
- The deformation of a 'simple' crest shape (e.g. oblique to lobe, lobe to asymmetrical lobe) is observed as a precursor to bedform interactions.
- Merging type I (cannibalization) typically followed defect creation and/or lateral linking.
- Superposition of defects was clearer on some dunes than on others, while the superposition remains present over prolonged time.
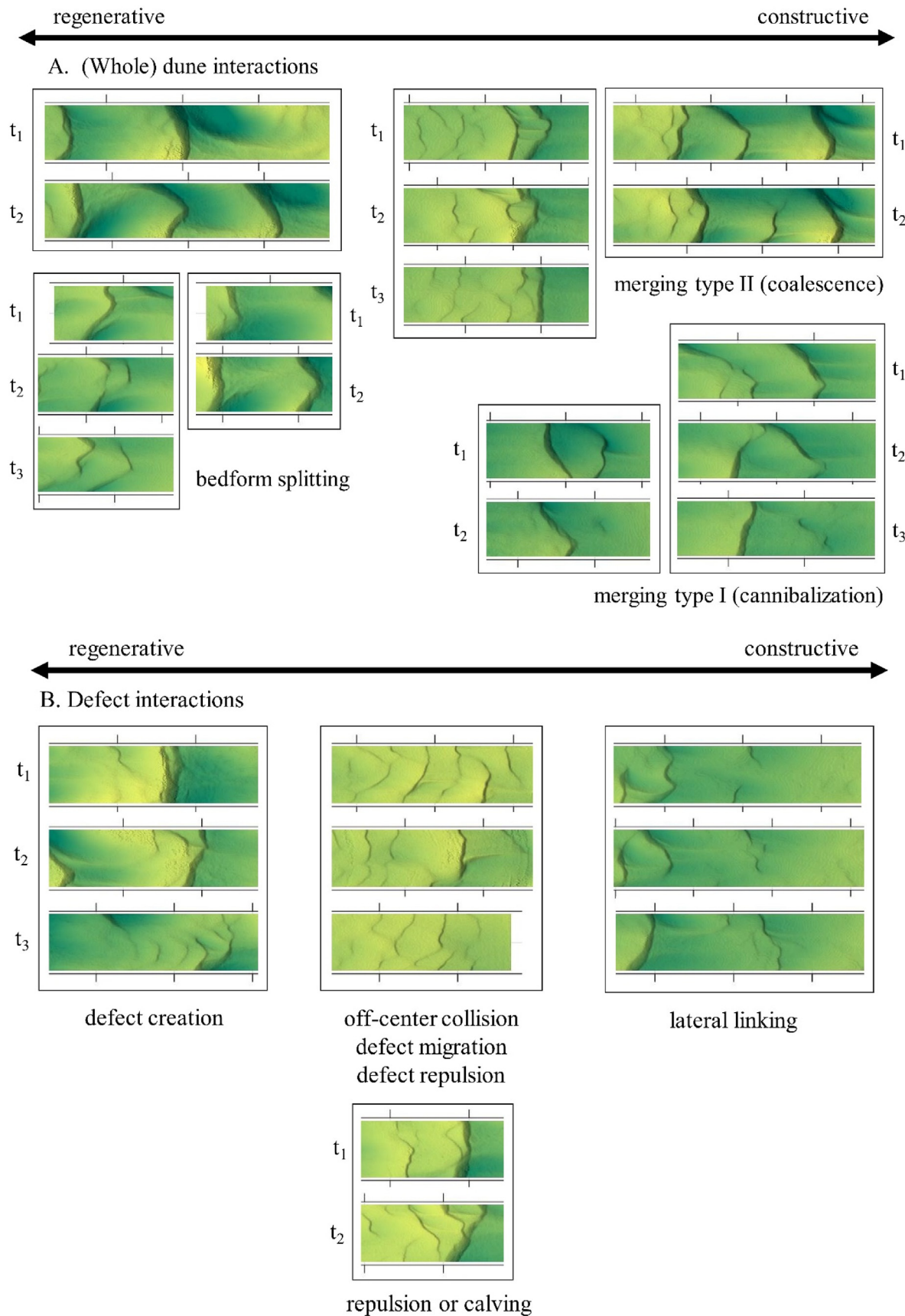
4.4. Dune migration tracking

The sediment flux from dune migration is determined by the dune height, the migration speed of the dune and the shape of the dune. For longitudinal transects (dune profiles), the difference in height between the trough and crest of a dune represents the dune height, and the migration speed is calculated from the crest distance travelled, divided by the elapsed time. The latter method works well when dunes are regularly spaced. In this case, there is little deformation between subsequent transects, with dunes easily identifiable between time steps. Fig. 8 illustrates dune tracking for an idealized situation, and for a situation in which the dune changes shape between time steps. For the idealized case, the positive difference between the two profiles (Δt) gives a rectangle, of which the two further corners approximate the net distance the dune migrated, with Δx and Δc being equal. For the non-idealized case, the dune deformed (e.g. higher crest and trough) between the two profiles and the migration distance based on the positive difference underestimates the distance the crest travelled. To determine the migration distance, dune height and interpretation of the dune height evolution, linking the dune troughs and crests in the different profiles is required.

The DEMs we collected are a detailed 3D representation of the dunes. Fig. 9 shows the dune crest migration in the longitudinal and cross-stream direction. The vectors are manually drawn and based on the net migration of dune crests. The five considered dunes show a variability in dune migration in the longitudinal and cross-stream direction, meaning crest migration speed varies for individual dunes, and between dunes. The difference in migration speed is due to shorter dunes traveling faster than longer dunes (Guala et al., 2014). The cross-stream and longitudinal variation in migration speed is higher than expected. DEMs of difference (DoD) from two DEMs automatically detect the variability in crest migration. Vectors mostly coincide with the blue areas that represent a positive difference in the DoD (Fig. 9). A discrepancy in the method arises when the time step is too large and consecutive dune crests exist in the same location. The time step for our measurements is 12 to 22 min, which was found as too large to automatically track all the dune crest migration processes, as especially short dunes changed substantially during that period. Determination of the dune sediment flux while (i) including the cross-stream component and (ii) involving active deformation into dune analyses remains problematic.

4.5. Comparison of dune migration tracking methods

In Fig. 10A and B, three methods to track dune migration are compared based on DoD, BTT and manual tracking. The methods confirm a high variability in dune migration speed of individual dunes along the centre line transect. The average crest migration speed, based on manual tracking, is 0.022 m/min. This aligns well with approximations obtained from BTT and the DoD. In Fig. 10C, the cross-stream variability as obtained with DoD is shown, with the middle transect deviating from the average migration speed of the dunes. Crest migration at the centre line transect is slower than the average migration speed of all transects. This suggests that the effect of 3D for dune crests and dune crest deformation cannot be neglected, not even in a narrow flume, such as used in the present study. For our data, there is no distinct relation between dune size and dune migration (Fig. 10D). The latter was also found by Jerolmack and Mohrig (2005a). A bed elevation between 0.08 and 0.12 m is observed for the experiments FR051515 and FR051522 with 0.15 m water depth, which is a 0.04 m range (Fig. 11). Lower or higher
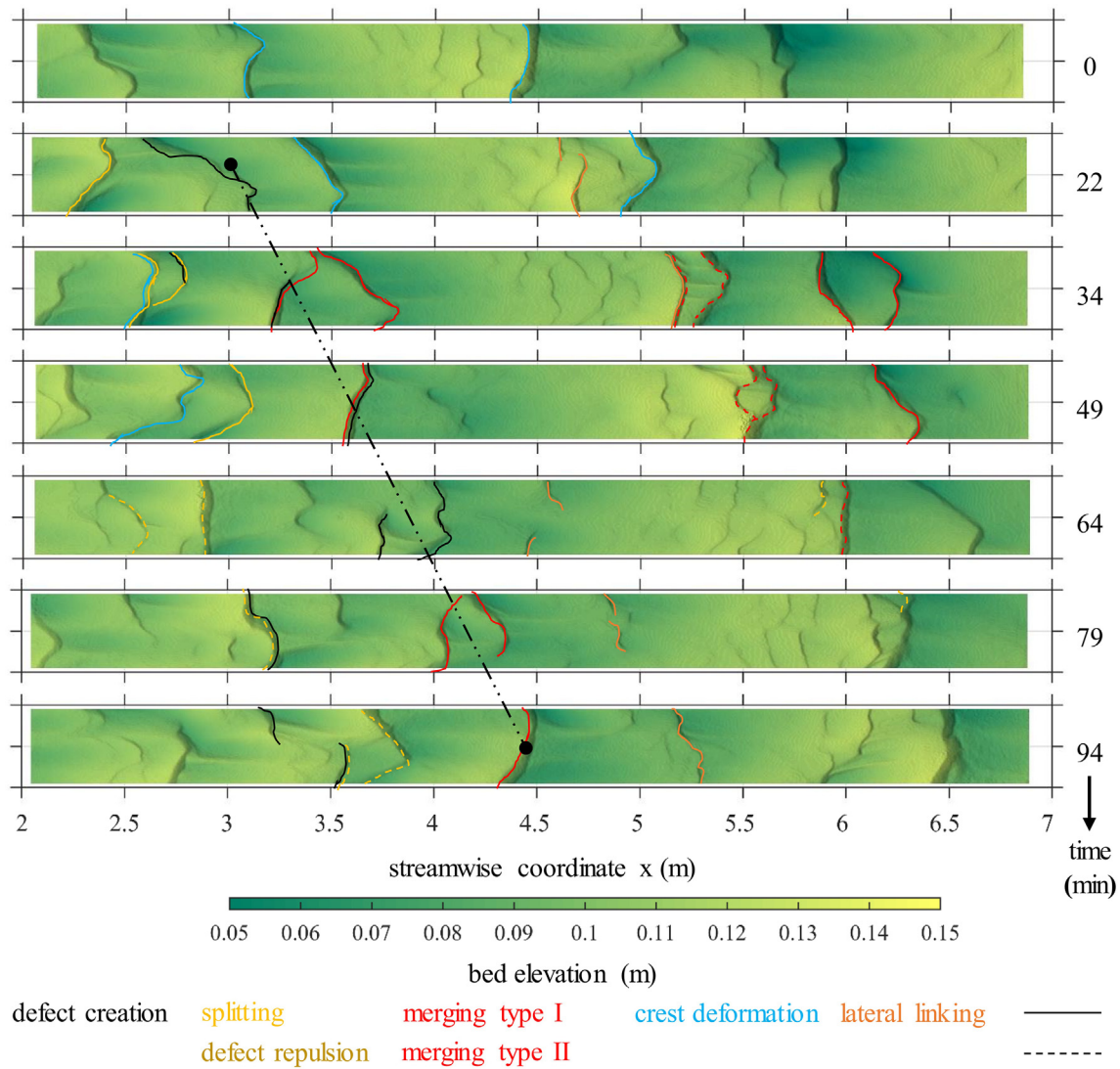
Fig. 5. Dune and defect interactions that were observed in five experiments with water depths of either 0.15 m or 0.18 m and average flow velocity of 0.5, 0.6 or 0.7 m/s. The processes are described in Table 1. Time steps between the DEMs are 12–17 min. The classification is based on Kocurek et al. (2010).

Fig. 6. Annotated topography of the sand bed of experiment FR051515. The DEMs cover 1 h 34 min of dune migration and evolution. Interpretation of dune migration and deformation processes are sketched in colour.

bed elevations, representing the tails, make up 10–20% of our bed elevation measurements. The average bed elevation is 0.03 m, which is lower than the range of bed elevations of 0.04 m. We conclude that crest migration of individual dunes varies in time and space (longitudinal and cross-sectional), using BBT and DoD to measure the variability. A limitation of BBT is that it is limited to transects, whilst the DoD can be applied in three dimensions, yet requires small time step between DEMs to work efficiently. Manual tracking outperforms both methods in accuracy, but is labour intensive. It is shown that the recorded dunes are typically irregular in shape and spacing, highlighting the existing challenges to analyse migration and active deformation in four dimensions, 3D topography changing over time.

4.6. Dune migration and active deformation

In this section, we explore the extent in which the dune and defect interactions contribute to variation in dune crest migration, based on manual tracking. In Fig. 12A, the crests of experiment FR051815 migrate at a velocity of ~0.01 m/min and dune interactions do not occur, except for defect interactions that were faster than could be tracked. The mean migration rate of the dunes is slow (Table 2) and an explanation is that the downstream dune, which is long and high (crest not visible),

interacts with the upstream neighbouring dune(s). Whereas the dune at x = 3 m is high and migrates slower, as more sediment needs to be redistributed to fill the trough region.

In the DEMs of experiment FR061815 (Fig. 12B), the crests migrate at velocities ranging from 0.02 to 0.06 m/min and average migration rate is higher, with dunes developed under faster flow conditions (Table 2, Fig. 8C). There are 3 dune crests that migrate at a stable pace, considerably slower than the two dune crests that undergo splitting and defect creation. Whilst one of the dunes accelerates, it creates 'space' for splitting downstream of the dune crest, and the dune crest deforms into a defect.

In the DEMs of experiment FR071515 (Fig. 12C), obtained under faster flow conditions (Fig. 8C), the first dune migrates at ~0.05 m/min, which is faster than the mean. Thereafter the dune merges (by cannibalization) and transforms into a defect, whilst the downstream dune migrates at only 0.03–0.04 m/min. The defect is likely to interact with the downstream crest, as the downstream dune crest moves slower than the mean. We observe that the dune crests that decelerate undergo crest deformation at the same time. Downstream of the merging dune, bedform splitting occurred. The newly formed dune migrates at 0.05 m/min, which is faster than the upstream crest migration speed of 0.03 m/min. The difference in speed between the latter creates 'space'
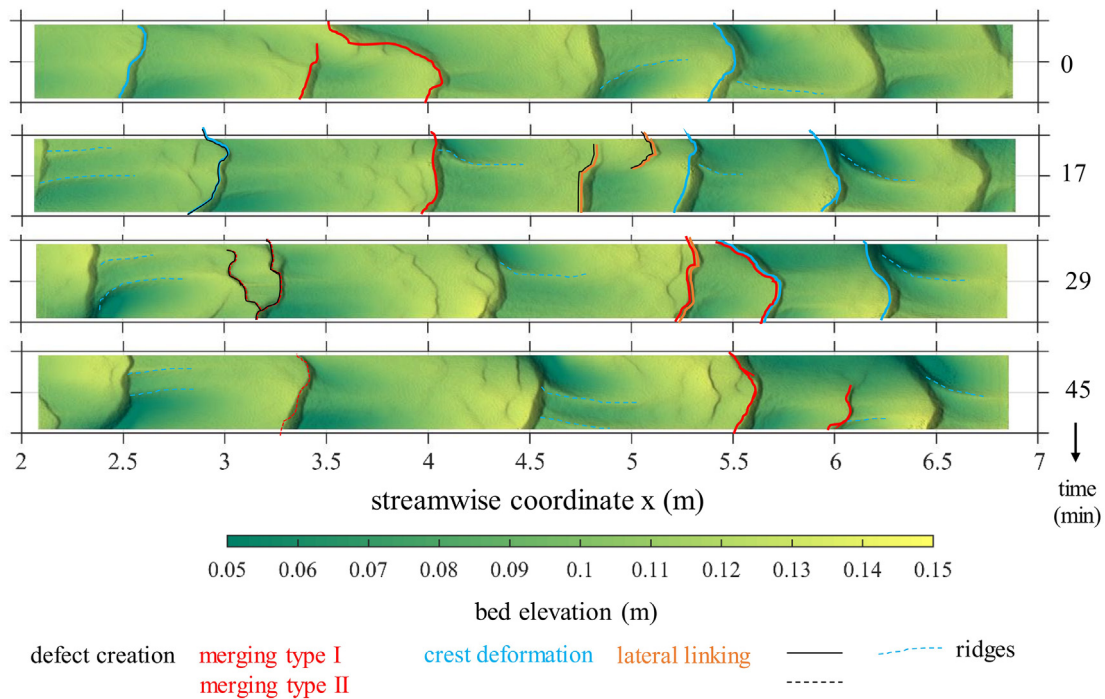
Fig. 7. Topography of the sand bed of experiment FR051522. The DEMs cover 45 min of dune migration and evolution. Interpretation of dune migration and deformation processes are sketched in colour.

for the newly formed dune. For the three experiments, we identified that dunes occasionally migrate at a constant velocity, but migration rates do not necessarily scale with the dune geometry. Variability in dune crest migration velocities exist, and phases of 'acceleration' and phases of 'deceleration' of dune crests occur. The fastest dune migration is observed when dune interactions occur, whereas the migration velocity of the upstream located dune is also affected. The upstream located dune migrates at a lower velocity when constructive dune interactions occur and thus 'provides space' for the newly formed dune.

5. Discussion

We provide solutions for using through-water images as a cost-effective method to obtain high resolution dune DEMs. The obtained maps of the sand bed are at a detail that has not been achieved previously. The method is highly suitable to measure the morphology of the sand bed, but awareness was raised by Woodget et al. (2015) that the visually stunning outputs are by no means error-free. Here, we compare our novel application of SfM on through-water images in the laboratory with other studies, and increase documentation on error sources in through-water SfM photogrammetry. Reesink et al. (2018) illustrate that sediment redistribution for steady-state deformation over and among dunes is pervasive and the same processes of sediment

redistribution are applicable to dunes that adapt to flow. Therefore, dunes are far more interconnected than has been commonly acknowledged by treating them as individual and measurable entities. In this work, the 3D character of dune and defect interactions is presented. The data set confirms the significant spatial and temporal variability, which is underestimated when merely considering 2D slices through dunes (Reesink et al., 2018). Following, we discuss the representativeness of our dune interaction measurements.

5.1. Validation of the DEMs

We used sand bed elevation measurements with laser scanner and in-air imagery to validate the obtained submerged bed elevation measurements. Laser scanner results exhibit lower point density and the capturing process was more time consuming, as also found by Morgan et al. (2017). We used the flume wall as bed elevation reference, aiding the initial processing of the SfM procedure to reproduce the sandy bed. We found it of importance to use seven GCPs per m^2. The SfM accuracy increased with increasing number of GCPs, at similar bed elevation across the point cloud. This step facilitated accurate approximation of the mean bed level and achieved that apparent depth was equal to the real depth at mean bed level. As a consequence, the water refraction correction scaled linearly with a deviation from the mean bed level. We found a factor of 1.2 for DEMs with an average water depth of 0.15 m, yet a factor of 1 for an average water depth of 0.18 m. Software updates during the study effected the point cloud results, and with the new release (4.2.26 to 4.4.12) a decreasing refraction correction was obtained for an average water depth of 0.15 m. We obtained the customized workflow through systematic trial and error, and a change in experimental setup requires renewed calibration and validation to guarantee accurate results.

5.2. Novel approach of through-water SfM

Agrafiotis et al. (2019) iteratively 'corrected' for the water refraction. In their results, apparent depth is equal to real depth at the mean bed

Table 5
Observations of dune interaction processes in experiment FR051515 and FR051522.

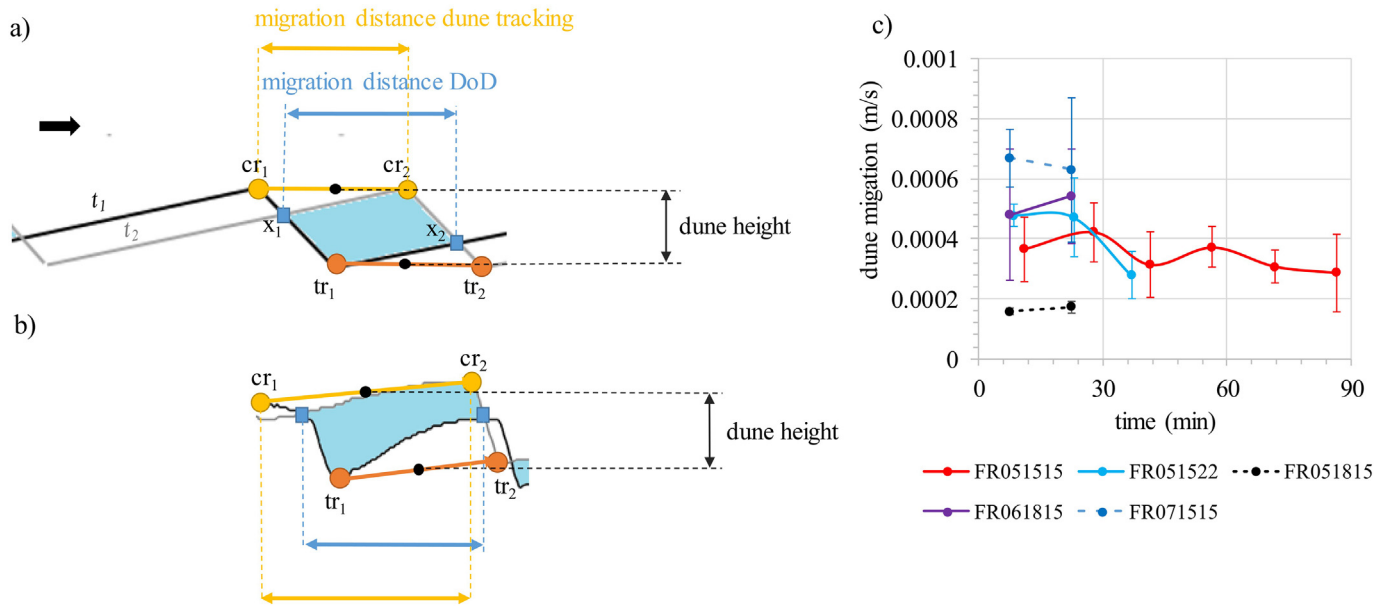|		FR051515	FR051522	Sum	Relative frequency (−)
Regenerative	Defect creation	3	2	5	0.28
	Defect repulsion	2		2	0.11
	Splitting	1		1	0.06
Constructive	Merging type I (cannibalization)	3	2	5	0.28
	Lateral linking	2	1	3	0.17
	Merging type II	1	1	2	0.11
		12	6	18	1.00

Fig. 8. Sketch showing the definition of migration length and dune height from dune profiles at t_1 and t_2 for an idealized situation (A) and for a dune that changed shape between t_1 and t_2 (B). The positive difference between the two profiles ($\Delta z > 0$ for Δt) is indicative of dune migration. (C) temporal variability in mean dune migration (manual tracking of crestlines).

level, and the refraction correction is linear (factor 1.5 to 1.6). Despite using different approaches and some major differences between their data set and our data set (water depth, camera height, and the ray-traveling percentages in water and air) there is agreement in the pattern of errors. Their individual photo refraction correction, explained and discussed in Skarlatos and Agrafiotis (2018), aims to develop a tool that is widely applicable (different flying heights, different depths, different seabed applications) and disregards camera coordinates. Our approach is different, as we apply a refraction correction on the point cloud that is simple and computationally inexpensive. Essential to our approach are accurate camera coordinates, submerged ground control points, and software calibration based on validation data. In our opinion, implementing the camera coordinates and underwater ground control points before initial processing is essential to obtain high accuracy: providing limits to the algorithms and thus guiding the iterative procedures. Our workflow can be improved by incorporating physics-based algorithms that represent the air-water refraction in SfM-MVS software.

We have shown in this study that our method is a novel application of through-water SfM, appropriate for shallow water conditions. We did not test our methodology on deeper water. Our approach compares to the correction approach of Westaway et al. (2001), without the need to model the water surface, and we omit extensive computation of refraction correction (Dietrich, 2017; Skarlatos and Agrafiotis, 2018) without significant loss of accuracy.

5.3. Dune interaction processes and crest deformation

The striking difference between present results and recent experiments of bed elevation measurements (Bradley and Venditti, 2019; Reesink et al., 2018; Tsubaki et al., 2018) is the high resolution of our maps and the addition of the 3D topographical information to the analysis. We identify common processes in subaqueous systems, such as bedform splitting, different types of merging, lateral linking and bedform/defect repulsion. Our bedform fields developed under stable
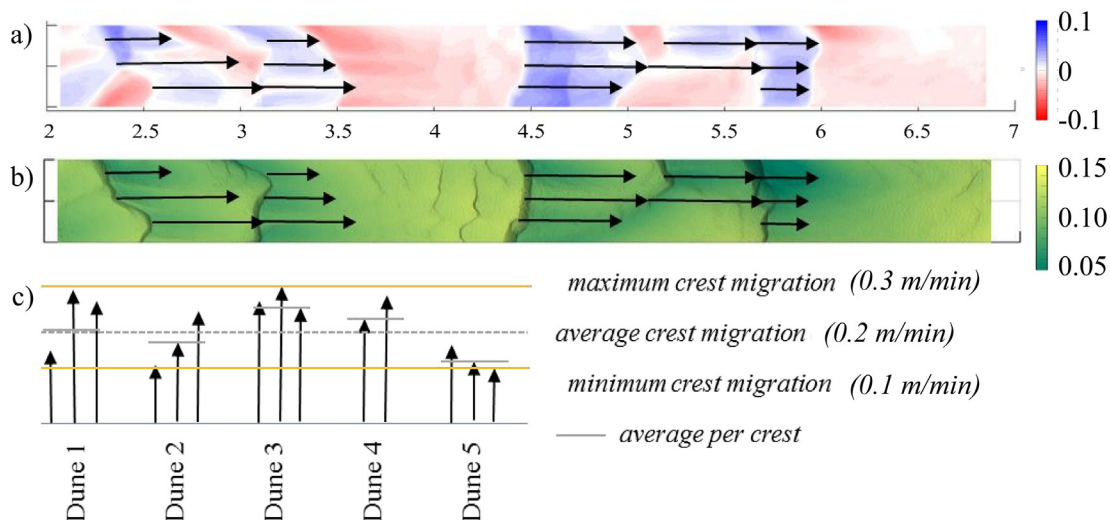

Fig. 9. vectors represent crest migration from 0 to 22 min of experiment FR051515. The net deposition (blue) in DEMs of difference (DoD) gives an indication of the crest migration, unless the time step is too long and crests occur in the same location. Crest migration varies in the cross-stream and streamwise direction.
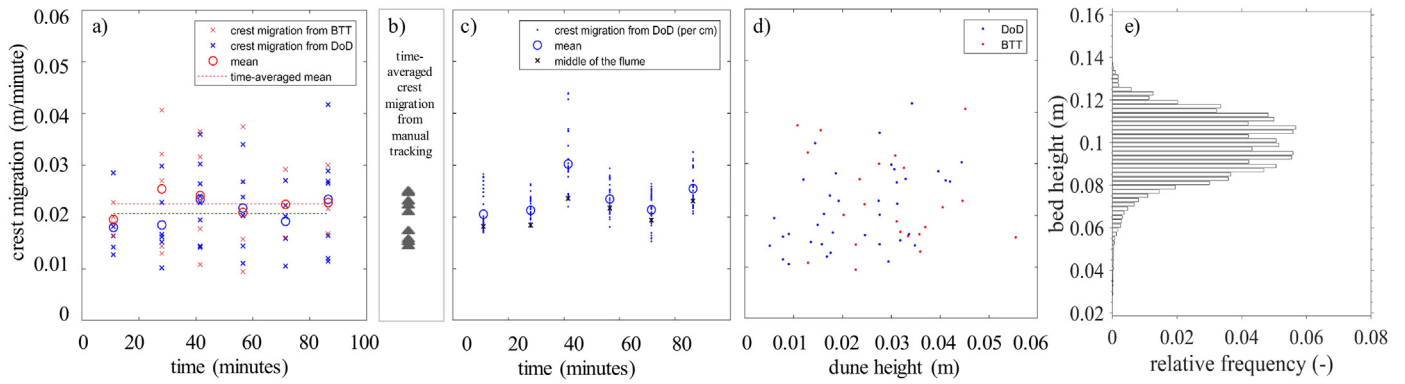
Fig. 10. Crest migration tracking. The migration of dunes in experiment FR051515 is shown for (A) the centre line transect and compares the net distance between crests of subsequent DEMs (DoD), the net movement of crests determined with BTT (van der Mark et al., 2008), and (B) from manual tracking. In (C) the method is applied along 36 longitudinal transects. In (D) the crest migration velocity against dune height is given.

boundary conditions and continued to show constructive and regenerative interactions at an equal distribution over 94 min of mapping (Table 5). This supports the statement that dunes continue to interact and jostle after achieving equilibrium (Coleman and Melville, 1996; Jerolmack and Mohrig, 2005b; Reesink et al., 2018). For experiments where only 3 to 4 DEMs were obtained, either regenerative or constructive processes were observed to be more abundant. This does not necessarily mean that those experiments were not representative of equilibrium conditions. Often there was not enough information to interpret dune interactions in the first and last map, as the duration required to identify regenerative and constructive interactions is longer than the measurement duration. Limited data are available on the frequency of dune interaction processes, and in our experiments merging and defect creation were most common (> 50%). Merging decreases the number of bedforms, and defect creation initializes creation of more bedforms. We showed that the processes relate to deformation of crest shapes. Simple crests are more frequently observed than irregular, sinuous or double crests. The simple shapes are classical sharp-crested dunes and the complex shapes are dunes in transition, possibly merging or affected by defects. The deformation of a 'simple' crest shape (e.g. oblique to lobe, lobe to asymmetrical lobe) is observed as a precursor to bedform interactions. The norm is a 3D simple dune crest, as a 2D dune crest is easily deformed when the crests come across the 2D shape. The data set, although limited in extent and dunes being

restricted by the flume walls, indicates that dune crests do not return to a 2D shape after transformation by bedform interactions. Multiple scales of dunes may exist (Frings and Kleinhans, 2008; Rubin and McCulloch, 1980), and our experiments are performed in shallow water and we thus consider a limited range of dunes. The setup is simple compared to real river beds, wherein a reach may exist of primary and secondary dunes, bars and bends. Notwithstanding, our observations are conceptually important, as they visualize how superimposed (smaller) bedforms affect the dynamics of (larger) dune crestlines. Cause and effect scenarios will be harder to assess when larger morphological elements (bars, bends) are present.

5.4. Dune interactions and the implication for sediment transport

The 23 obtained DEMs for six experiments identify nearly all processes from the framework of Kocurek et al. (2010). In order to classify defect interactions, a higher recording frequency is required, as we observed defect interactions to be faster than whole bedform interactions. This is due to less sediment displacement for defect interactions than for bedform interactions, and thus the process is faster. Nevertheless, we were able to identify a cascade of processes: e.g. merging of upstream dunes coincides with defect creation at downstream dunes, the defect later merges with the downstream crest whilst calving (or repulsion) is observed on the downstream dune. The information 3D SfM provides
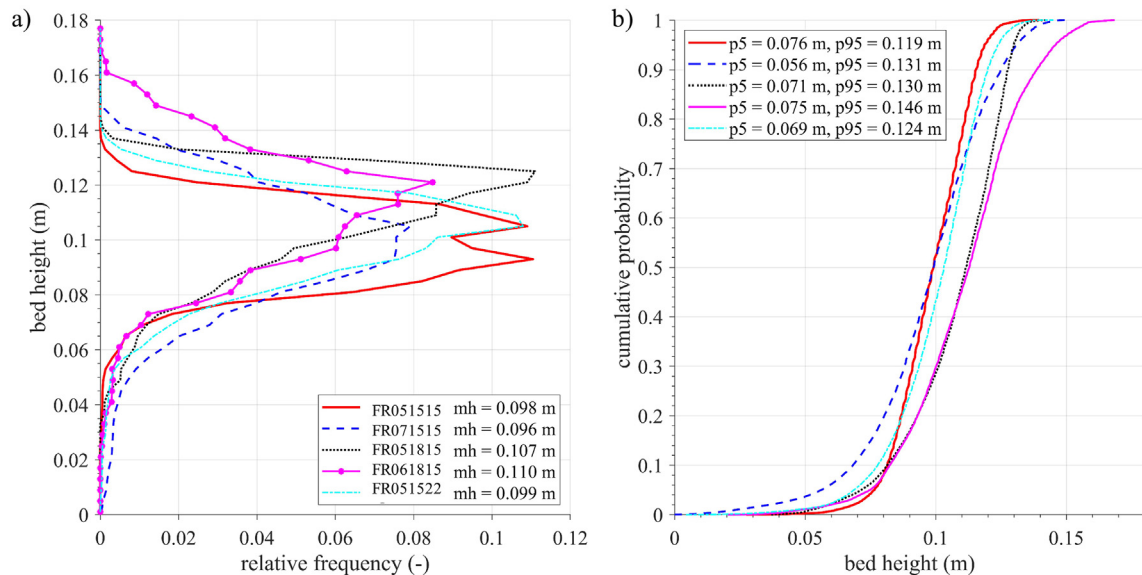

Fig. 11. Bed height distribution of the experiments with mean bed height (mh), 5th percentile (p5) and 95th percentile (p95). Zero elevation is the flume floor and the initial bed level is 0.105 m.
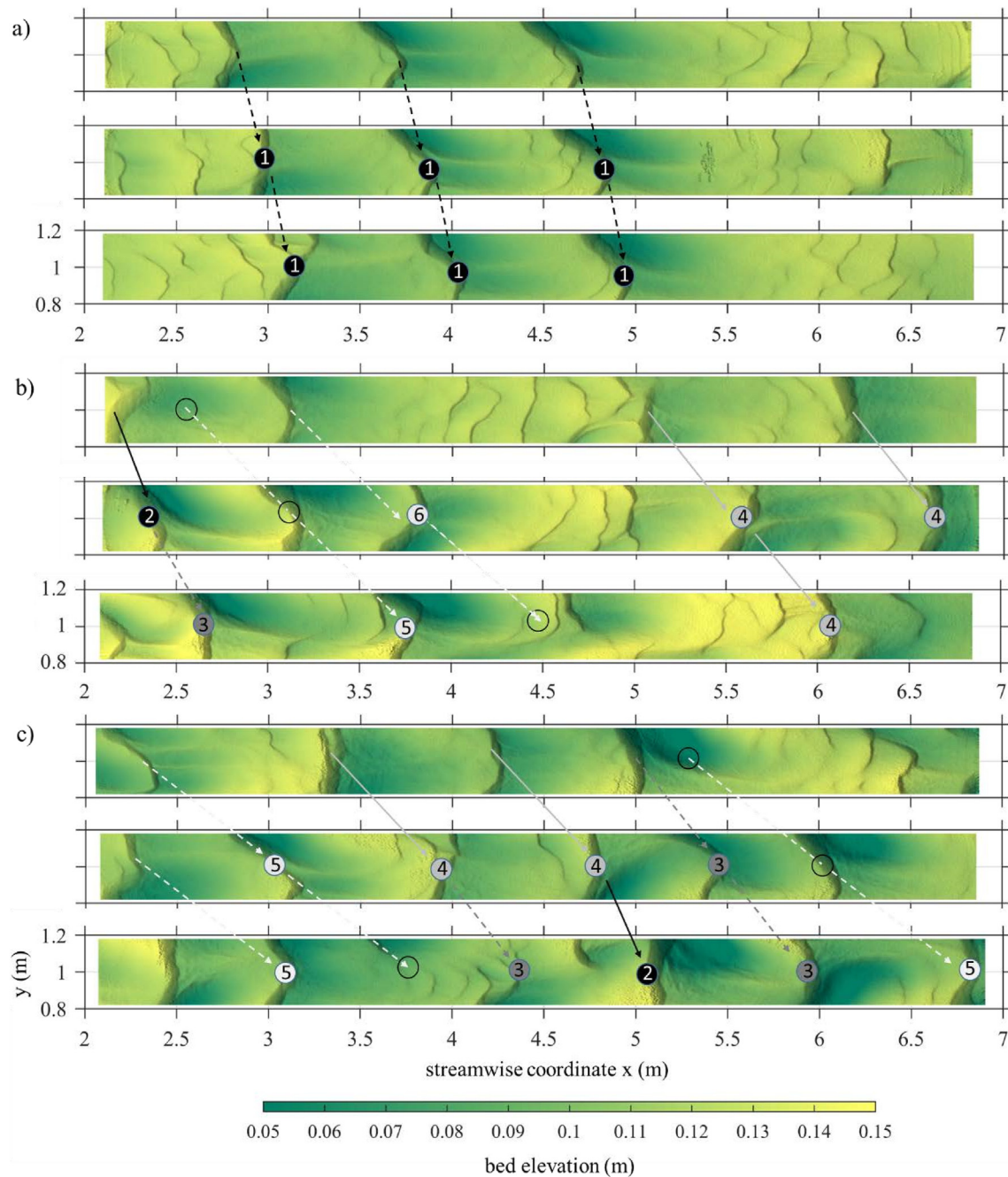
Fig. 12. The migration velocity of crests for experiments FR051815 (A), FR061815 (B) and FR071515 (C). The numbers in the circles give migration velocity in cm/min. Empty circles are used for newly generated crests and vanished crests.

is necessary to identify this cascade of dune interactions. Classifying dune interactions is subjective to interpretation as (1) a temporal information gap must be filled and (2) due to cascades of interactions. The interactions between neighbouring dunes appear messy initially, with the framework of Kocurek et al. (2010) aiding strongly in recognizing the patterns. We observe that at the dune scale, dune crests accelerate and decelerate as they are undergoing change (shown in Fig. 12). An important part of the variability in dune migration velocities measured in Fig. 10 can be explained by dune interactions. The temporal component of the underlying sediment transport processes is little understood in relation to average transport. Our high-resolution maps and DoDs allow to quantify how much sediment is being redistributed locally (dune-averaged transport and deformation fluxes), with the sediment flux measurements not intruding the bed or flow. We show that this

type of measurement is needed. However, a higher mapping frequency is also required, which is recommended for future work.

6. Conclusions

In this study, dune field DEMs with a high level of detail were obtained with through-water images and SfM tools. We show that such a dataset is needed to improve our understanding of complex dune interactions. Our novel application of SfM processing of through-water images results in an air-water refraction corrected DEM. We presented a workflow, which requires the determination of internal camera parameters, the geo-location of camera positions and incorporation of 3D GCPs. We obtained mapped DEMs of an accuracy of 1.5 points per mm^2 and presented their plots when interpolated onto a 2 mm grid

× 2 mm grid. Our through-water SfM data are consistent with data obtained from in-air SfM and laser scanner measurements. Linear correction of the bed elevation, to allow for refraction from the air-water interface, is needed for some of the DEMs, depending on the camera set-up.

Numerous dune and defect interactions are identified for the dune fields in our experimental tests, such as bedform splitting, different types of merging, lateral linking and bedform/defect repulsion. Crest deformation often indicates the start of dune interaction. A 2D straight crest is susceptible to defect interactions and the crest shape deforms easily. Superposed features are dominant over large (long) dunes. Superposition remains present for prolonged time, with observed superposition dynamics being faster than the temporal resolution of our measurements. Crest migration varies between individual dunes and in time. Dune interactions add to the variability in dune crest migration, and we observe an increased migration rate as onset to various dune deformation processes, e.g. bedform splitting. Whilst neighbouring dunes tend to slow down or accelerate. We identify a cascade of processes and show that 3D DEMs at high frequency are required to resolve observed rapid deformations and interaction of dunes. Notwithstanding the simplification of flume experiments compared to real river beds, our observations are conceptually important to assess what is 'normal' dune behaviour and to quantify the temporal effect of dune interactions on energy decay and sediment transport, which will be harder to assess when larger morphological elements (bars, bends) are present.

Declaration of competing interest

The authors declare that they have no known competing financial interests or personal relationships that could have appeared to influence the work reported in this paper.

Acknowledgements

References

Abraham, D., Kuhnle, R.A., Odgaard, A.J., 2011. Validation of bed-load transport measurements with time-sequenced bathymetric data. J. Hydraul. Eng. 137, 723–728. https://doi.org/10.1061/(ASCE)HY.1943-7900.0000357.

Agrafiotis, P., Drakonakis, G.I., Georgopoulos, A., Skarlatos, D., 2017. The effect of underwater imagery radiometry on 3D reconstruction and orthoimagery. Int. Arch. Photogramm. Remote Sens. Spat. Inf. Sci., pp. 25–31. https://doi.org/10.5194/isprs-archives-XLII-2-W3-25-2017

Agrafiotis, P., Skarlatos, D., Georgopoulos, A., Karantzalos, K., 2019. DepthLearn: learning to correct the refraction on point clouds derived from aerial imagery for accurate dense shallow water bathymetry based on SVMs-fusion with LiDAR point clouds. Remote Sens., 11 https://doi.org/10.3390/rs11192225.

Alho, P., Kukko, A., Hyyppä, H., Kaartinen, H., Hyyppä, J., Jaakkola, A., 2009. Application of boat-based mobile laser scanning for river survey. ESPL 34, 1831–1838. https://doi.org/10.1002/esp.1879.

Best, J., 2005. The fluid dynamics of river dunes: a review and some future research directions. J. Geophys. Res. Earth 110. https://doi.org/10.1029/2004JF000218.

Blom, A., Ribberink, J.S., De Vriend, H.J., 2003. Vertical sorting in bed forms: flume experiments with a natural and a trimodal sediment mixture. Water Resour. Res. 39, ESG11–ESG113.

Bradley, R.W., Venditti, J.G., 2019. Transport scaling of dune dimensions in shallow flows. J. Geophys. Res. Earth 124, 526–547. https://doi.org/10.1029/2018JF004832.

Coleman, S.E., Melville, B.W., 1996. Initiation of bed forms on a flat sand bed. J. Hydraul. Eng. 122, 301–309.

Dey, S. (2014). Turbulence in open-channel flows. In S. Dey (Ed.), Fluvial Hydrodynamics: Hydrodynamic and Sediment Transport Phenomena (pp. 95–187). Berlin, Heidelberg: Springer Berlin Heidelberg.

Dietrich, J.T., 2017. Bathymetric Structure-from-Motion: extracting shallow stream bathymetry from multi-view stereo photogrammetry. ESPL 42, 355–364. https://doi.org/10.1002/esp.4060.

Fathel, S.L., Furbish, D.J., Schmeeckle, M.W., 2015. Experimental evidence of statistical ensemble behavior in bed load sediment transport. J. Geophys. Res. Earth 120, 2298–2317. https://doi.org/10.1002/2015JF003552.

Ferreira, E., Chandler, J., Wackrow, R., Shiono, K., 2017. Automated extraction of free surface topography using SfM-MVS photogrammetry. Flow Meas. Instrum. 54, 243–249. https://doi.org/10.1016/j.flowmeasinst.2017.02.001.

Friedrich, H., Paarlberg, A.J., Lansink, J., 2008. Evaluation of statistical properties of dune profiles. Proc. of the 5th IAHR Symposium on River, Coastal and Estuarine Morphodynamics (RCEM 2007), pp. 913–921.

Frings, R.M., Kleinhans, M.G., 2008. Complex variations in sediment transport at three large river bifurcations during discharge waves in the river Rhine. Sedimentology 55, 1145–1171. https://doi.org/10.1111/j.1365-3091.2007.00940.x.

Fryer, J.G., 1983. A simple system for photogrammetric mapping in shallow water. Photogramm. Rec. 11, 203–208. https://doi.org/10.1111/j.1477-9730.1983.tb00471.x.

Guala, M., Singh, A., Badheartbull, N., Foufoula-Georgiou, E., 2014. Spectral description of migrating bed forms and sediment transport. J. Geophys. Res. Earth 119, 123–137. https://doi.org/10.1002/2013JF002759.

Heays, K.G., Friedrich, H., Melville, B.W., Nokes, R., 2014. Quantifying the dynamic evolution of graded gravel beds using particle tracking velocimetry. J. Hydraul. Eng. 140. https://doi.org/10.1061/(ASCE)HY.1943-7900.0000850.

Javernick, L., Brasington, J., Caruso, B., 2014. Modeling the topography of shallow braided rivers using Structure-from-Motion photogrammetry. Geomorphology 213, 166–182. https://doi.org/10.1016/j.geomorph.2014.01.006.

Jerolmack, D.J., & Mohrig, D. (2005a). Interactions between bed forms: Topography, turbulence, and transport. *J Geophys Res-Earth, 110*, DOI: https://doi.org/10.1029/2004JF000126.

Jerolmack, D.J., Mohrig, D., 2005b. A unified model for subaqueous bed form dynamics. Water Resour. Res. 41, 1–10. https://doi.org/10.1029/2005WR004329.

Julien, P.Y., Klaassen, G.J., 1995. Sand-dune geometry of large rivers during floods. J. Hydraul. Eng. 121, 657–663. https://doi.org/10.1061/(ASCE)0733-9429(1995)121:9(657).

Kasvi, E., Salmela, J., Lotsari, E., Kumpula, T., Lane, S.N., 2019. Comparison of remote sensing based approaches for mapping bathymetry of shallow, clear water rivers. Geomorphology 333, 180–197. https://doi.org/10.1016/j.geomorph.2019.02.017.

Kinzel, P.J., Wright, C.W., Nelson, J.M., Burman, A.R., 2007. Evaluation of an experimental LiDAR for surveying a shallow, braided, sand-bedded river. J. Hydraul. Eng. 133, 838–842. https://doi.org/10.1061/(ASCE)0733-9429(2007)133:7(838).

Kleinhans, M.G., Wilbers, A.W.E., ten Brinke, W.B.M., 2007. Opposite hysteresis of sand and gravel transport upstream and downstream of a bifurcation during a flood in the River Rhine, the Netherlands. Neth. J. Geosci. 86, 273–285.

Kocurek, G., Ewing, R.C., Mohrig, D., 2010. How do bedform patterns arise? New views on the role of bedform interactions within a set of boundary conditions. ESPL 35, 51–63. https://doi.org/10.1002/esp.1913.

Kwoll, E., Venditti, J.G., Bradley, R.W., Winter, C., 2017. Observations of coherent flow structures over subaqueous high- and low-angle dunes. J. Geophys. Res. Earth 122, 2244–2268. https://doi.org/10.1002/2017JF004356.

Lane, S.N., Richards, K.S., Chandler, J.H., 1994. Developments in monitoring and modelling small-scale river bed topography. ESPL 19, 349–368. https://doi.org/10.1002/esp.3290190406.

Lane, S.N., Westaway, R.M., Hicks, D.M., 2003. Estimation of erosion and deposition volumes in a large, gravel-bed, braided river using synoptic remote sensing. ESPL 28, 249–271. https://doi.org/10.1002/esp.483.

Lane, S.N., Widdison, P.E., Thomas, R.E., Ashworth, P.J., Best, J.L., Lunt, I.A., Sambrook Smith, G.H., Simpson, C.J., 2010. Quantification of braided river channel change using archival digital image analysis. ESPL 35, 971–985. https://doi.org/10.1002/esp.2015.

Lau, Y.L., Krishnappan, B.G., 1985. Sediment transport under ice cover. J. Hydraul. Eng. 111, 934–950. https://doi.org/10.1061/(ASCE)0733-9429(1985)111:6(934).

Lavest, J.M., Rives, G., Lapresté, J.T., 2003. Dry camera calibration for underwater applications. Mach. Vis. Appl. 13, 245–253. https://doi.org/10.1007/s00138-002-0112-z.

Lefebvre, A., 2019. Three-dimensional flow above river bedforms: insights from numerical modeling of a natural dune field (Río Paraná, Argentina). J. Geophys. Res. Earth https://doi.org/10.1029/2018JF004928.

Lefebvre, A., Paarlberg, A.J., Winter, C., 2016. Characterising natural bedform morphology and its influence on flow. Geo-Mar. Lett. 36, 379–393. https://doi.org/10.1007/s00367-016-0455-5.

Li, W., Gee, T., Delmas, P., & Friedrich, H. (2016). Evaluating using GoPro cameras and Tsai's calibration for video-based submerged river-bed reconstruction. In, Proc. of International Conference Image and Vision Computing New Zealand. DOI: https://doi.org/10.1109/IVCNZ.2016.7804465.

van der Mark, C.F., Blom, A., Hulscher, S.M.J.H., 2008. Quantification of variability in bedform geometry. J. Geophys. Res. Earth 113. https://doi.org/10.1029/2007JF000940.

Matthes, G.H., 1947. Macroturbulence in natural stream flow. EOS Trans. Am. Geophys. Union 28, 255–265. https://doi.org/10.1029/TR028i002p00255.

McElroy, B., Mohrig, D., 2009. Nature of deformation of sandy bed forms. J. Geophys. Res. Solid Earth, 114 https://doi.org/10.1029/2008JF001220.

Moore, E.J., 1976. Underwater photogrammetry. Photogramm. Rec. 8, 748–763. https://doi.org/10.1111/j.1477-9730.1976.tb00852.x.

Morgan, J.A., Brogan, D.J., Nelson, P.A., 2017. Application of Structure-from-Motion photogrammetry in laboratory flumes. Geomorphology 276, 125–143. https://doi.org/10.1016/j.geomorph.2016.10.021.

Mosbrucker, A.R., Major, J.J., Spicer, K.R., Pitlick, J., 2017. Camera system considerations for geomorphic applications of SfM photogrammetry. ESPL https://doi.org/10.1002/esp.4066 (n/a-n/a).

Nittrouer, J.A., Allison, M.A., Campanella, R., 2008. Bedform transport rates for the lower-most Mississippi River. J. Geophys. Res. Earth 113. https://doi.org/10.1029/2007JF000795.

Parsons, D.R., Best, J.L., Orfeo, O., Hardy, R.J., Kostaschuk, R., Lane, S.N., 2005. Morphology and flow fields of three-dimensional dunes, Rio Paraná, Argentina: results from simultaneous multibeam echo sounding and acoustic Doppler current profiling. J. Geophys. Res. Earth, 110 https://doi.org/10.1029/2004JF000231.

Qin, J., Wu, T., Zhong, D.Y., 2015. Spectral behavior of gravel dunes. Geomorphology 231, 331–342. https://doi.org/10.1016/j.geomorph.2014.12.023.

Reesink, A.J.H., Parsons, D.R., Ashworth, P.J., Best, J.L., Hardy, R.J., Murphy, B.J., McLelland, S.J., Unsworth, C., 2018. The adaptation of dunes to changes in river flow. Earth Sci. Rev. 185, 1065–1087. https://doi.org/10.1016/j.earscirev.2018.09.002.

Rubin, D.M., McCulloch, D.S., 1980. Single and superimposed bedforms: a synthesis of San Francisco Bay and flume observations. Sediment. Geol. 26, 207–231. https://doi.org/10.1016/0037-0738(80)90012-3.

Shortis, M., 2015. Calibration techniques for accurate measurements by underwater camera systems. Sensors 15, 30810–30827. https://doi.org/10.3390/s151229831.

Simons, D.B., Richardson, E.V., Nordin, C.F., 1965. Bedload Equation for Ripples and Dunes.

Singh, A., Foufoula-Georgiou, E., 2013. Effect of Migrating Bed Topography on Flow Turbulence: Implications for Modelling Sediment Transport. pp. 323–339.

Skarlatos, D., Agrafiotis, P., 2018. A novel iterative water refraction correction algorithm for use in Structure from Motion photogrammetric pipeline. J. Mar. Sci. Eng. 6, 77.

Terwisscha van Scheltinga, R.C., Friedrich, H., Coco, G., 2019. Sand particle velocities over a subaqueous dune slope using high-frequency image capturing. ESPL https://doi.org/10.1002/esp.4617.

Tsubaki, R., Baranya, S., Muste, M., Toda, Y., 2018. Spatio-temporal patterns of sediment particle movement on 2D and 3D bedforms. Exp. Fluids 59. https://doi.org/10.1007/s00348-018-2551-y.

Venditti, J.G., Bennett, S.J., 2000. Spectral analysis of turbulent flow and suspended sediment transport over fixed dunes. J. Geophys. Res. Oceans 105, 22035–22047.

Venditti, J.G., Church, M., Bennett, S.J., 2005. Morphodynamics of small-scale superimposed sand waves over migrating dune bed forms. Water Resour. Res. 41. https://doi.org/10.1029/2004WR003461 (W10423-10421-W10423-10414).

Venditti, J.G., Lin, C.Y.M., Kazemi, M., 2016. Variability in bedform morphology and kinematics with transport stage. Sedimentology 63, 1017–1040. https://doi.org/10.1111/sed.12247.

Warmink, J.J., Dohmen-Janssen, C.M., Lansink, J., Naqshband, S., van Duin, O.J.M., Paarlberg, A.J., Termes, P., Hulscher, S.J.M.H., 2014. Understanding river dune splitting through flume experiments and analysis of a dune evolution model. ESPL 39, 1208–1220. https://doi.org/10.1002/esp.3529.

Werner, B.T., Kocurek, G., 1997. Bed-form dynamics: does the tail wag the dog? Geology 25, 771–774. https://doi.org/10.1130/0091-7613(1997)025<0771:BFDDTT>2.3.CO;2.

Westaway, R.M., Lane, S.N., Hicks, D.M., 2001. Remote sensing of clear-water, shallow, gravel-bed rivers using digital photogrammetry. Photogramm. Eng. Remote. Sens. 67, 1271–1281.

Westoby, M.J., Brasington, J., Glasser, N.F., Hambrey, M.J., Reynolds, J.M., 2012. 'Structure-from-Motion' photogrammetry: a low-cost, effective tool for geoscience applications. Geomorphology 179, 300–314. https://doi.org/10.1016/j.geomorph.2012.08.021.

Wilbers, A.W.E., Ten Brinke, W.B.M., 2003. The response of subaqueous dunes to floods in sand and gravel bed reaches of the Dutch Rhine. Sedimentology 50, 1013–1034. https://doi.org/10.1046/j.1365-3091.2003.00585.x.

Woodget, A.S., Carbonneau, P.E., Visser, F., Maddock, I.P., 2015. Quantifying submerged fluvial topography using hyperspatial resolution UAS imagery and structure from motion photogrammetry. ESPL 40, 47–64. https://doi.org/10.1002/esp.3613.